PAPER

Photo-induced reactions from efficient molecular dynamics with electronic transitions using the FIREBALL local-orbital density functional theory formalism

IOP Publishing Journal of Physics: Condensed Matter
J. Phys.: Condens. Matter **27** (2015) 175002 (11pp) doi:10.1088/0953-8984/27/17/175002

Photo-induced reactions from efficient molecular dynamics with electronic transitions using the FIREBALL local-orbital density functional theory formalism

Vladimír Zobač[1,2], James P Lewis[1,3], Enrique Abad[4], Jesús I Mendieta-Moreno[5], Prokop Hapala[1], Pavel Jelínek[1,6] and José Ortega[5]

[1] Institute of Physic, Academy of Sciences of the Czech Republic, Cukrovarnická 10, CZ-16200 Prague, Czech Republic
[2] Department of Physical Electronics, Faculty of Nuclear Sciences and Physical Engineering, Czech Technical University in Prague, Czech Republic
[3] Department of Physics and Astronomy, West Virginia University, Morgantown WV 26506, USA
[4] Computational Biochemistry Group, Institute of Theoretical Chemistry, University of Stuttgart, Pfaffenwaldring 55 70569 Stuttgart, Germany
[5] Departamento de Física Teórica de la Materia Condensada and Condensed Matter Physics Center (IFIMAC), Universidad Autónoma de Madrid, ES-28049 Madrid, Spain
[6] Graduate School of Engineering, Osaka University 2-1, Yamada-Oka, Suita, Osaka 565-0871, Japan

E-mail: james.lewis@mail.wvu.edu, jelinekp@fzu.cz and jose.ortega@uam.es

Received 4 January 2015, revised 12 February 2015
Accepted for publication 20 February 2015
Published 20 March 2015

Abstract

The computational simulation of photo-induced processes in large molecular systems is a very challenging problem. Firstly, to properly simulate photo-induced reactions the potential energy surfaces corresponding to excited states must be appropriately accessed; secondly, understanding the mechanisms of these processes requires the exploration of complex configurational spaces and the localization of conical intersections; finally, photo-induced reactions are probability events, that require the simulation of hundreds of trajectories to obtain the statistical information for the analysis of the reaction profiles. Here, we present a detailed description of our implementation of a molecular dynamics with electronic transitions algorithm within the local-orbital density functional theory code FIREBALL, suitable for the computational study of these problems. As an example of the application of this approach, we also report results on the [2 + 2] cycloaddition of ethylene with maleic anhydride and on the [2 + 2] photo-induced polymerization reaction of two C_{60} molecules. We identify different deactivation channels of the initial electron excitation, depending on the time of the electronic transition from LUMO to HOMO, and the character of the HOMO after the transition.

Keywords: density functional theory, non-adiabatic molecular dynamics, local-orbital basis set, photo-induced cycloaddition

(Some figures may appear in colour only in the online journal)

1. Introduction

One of the greatest challenges in simulation methodology is to accurately and efficiently interpret photo-induced reaction mechanisms which are critically important in many chemical processes, such as vision, photodamage, UV absorption, photosynthesis, photography, etc. In Born–Oppenheimer (or adiabatic) molecular dynamics—the nuclei follow classical

trajectories defined on a single potential energy surface (PES); this PES corresponds to the ground state electronic energy of the system, for frozen atomic configurations. To accurately simulate photo-induced reactions, the excited potential energy surface must be appropriately accessed beyond the Born–Oppenheimer approximation. Additionally, the ability of the electron to transition between the ground PES and the excited PES in the region close to the conical intersection between the two PESs is very important in accurately portraying the transition that will occur in photo-induced reactions.

Photo-induced processes in large molecular systems are computationally intensive to simulate due to the complexities in modelling the vast search space associated with photo-activated reaction mechanisms. Also, the search for conical intersections is quite more complex than geometry optimization [1–4]. Photo-induced polymerization reactions, such as the photo-induced [2 + 2] cycloaddition reactions of two C_{60} molecules, would easily require large simulation systems containing hundreds of atoms. Biological photo-induced reactions are even more demanding in computational resources [5]. Additionally, photo-induced reaction mechanisms are probability events. Hence, to accurately simulate reaction mechanisms, hundreds, if not thousands, of trajectories are required to obtain the proper statistical information. Thus, efficient algorithms are needed, at least, at an exploratory level. There is a definitive need for simulation tools that can, at minimum, obtain sufficiently accurate results that will efficiently yield significant insight in photo-induced reaction mechanisms without overburdening computational resources.

Broadly speaking, two types of non-adiabatic methods dominate the literature: Ehrenfest Dynamics (ED) methods and surface hopping (SH) methods [6–8]. In the ED approach, the nuclei move classically on a single effective PES obtained by averaging over all the adiabatic states involved; however, in SH methods the classical degrees of freedom (nuclei coordinates) evolve on single adiabatic surfaces [6], and make probabilistic hops from one PES to another. Surface-Hopping methods present key advantages over ED methods, because the system is always on a certain pure adiabatic state, not in an average non-physical state. Moreover, ED calculations sometimes lead to non-physical features, such as energetically inaccessible levels populated or violation of microscopic reversibility [9]. Tully's molecular dynamics with electronic transitions (MDET) algorithm [10] employes a surface hopping strategy [11] to switch between different adiabatic states. In Tully's MDET approach, the system evolves on one of the PES corresponding to a particular adiabatic state E_A of the system. Using the idea of ensemble of trajectories, the transitions between different PES are determined through a probabilistic approach; in particular, the transitions between adiabatic electronic states are determined using the *fewest-switches algorithm* that considers the minimum number of non-adiabatic transitions that are compatible with the correct statistical distribution of state populations at all times. The MDET method is probably the most used and successful method to deal with problems in which coupling between electrons and ions is required.

The most efficient first-principles molecular dynamics (MD) approaches are based on density functional theory (DFT). In recent years the MDET approach has been implemented using DFT and applied to several problems [9, 12–24]. Our goal is to target large-scale photo-polymerization trajectory ensembles that include several hundreds of atoms and explore several hundreds of trajectories. As such, we have focused primarily on implementing a MDET algorithm within FIREBALL, an efficient local-orbital DFT MD technique [25]. We have previously demonstrated a successful application of the FIREBALL DFT–MDET in the photo-isomerization processes of stilbene and azobenzene [19].

The remainder of this paper is organized as follows. In section 2, we present a detailed description of our implementation of DFT–MDET within the FIREBALL code. In section 3, we present results for two different photo-induced cycloaddition reactions: the [2 + 2] cycloaddition of ethylene with maleic anhydride to form cyclobutane-1-2-dicarboxilic anhydride and the [2 + 2] photo-induced polymerization reaction of two C_{60} molecules. Finally, in section 4, we summarize the main conclusions.

2. Description of the method

2.1. Local-orbital DFT: FIREBALL

FIREBALL [25–29] is an efficient simulation DFT package that is specifically designed for the study of complex systems using MD simulations. The main characteristics of FIREBALL are: (i) basis sets of short-range numerical atomic-like orbitals [26, 30]; (ii) the technique is completely formulated in *real-space* (no need for supercells) and does not require the use of grids for the charge density and potential calculations; (iii) self-consistency is achieved using the orbital occupation numbers [27] ; (iv) a practical tabulation-interpolation scheme is used so that all the interactions/integrals required during the MD simulation can be calculated beforehand and stored in data-tables [26], speeding up the calculations.

In this approach, the energy functional is written as:

$$E_{\rm tot}[\rho(\mathbf{r})] = E_{\rm BS} - E_{ee}[\rho(\mathbf{r})] + E_{xc}[\rho(\mathbf{r})] - \int \rho(\mathbf{r}) V_{xc}[\rho(\mathbf{r})]\,{\rm d}^3r + E_{\rm ion-ion}. \quad (1)$$

where $\rho(\mathbf{r})$ is the *input* electron density [31, 32], which is determined in a selfconsistent way in terms of the orbital occupation numbers [27, 33, 34] , see below. $E_{\rm BS}$ is a sum over occupied eigenvalues, $E_{\rm BS} = \sum_{i\in{\rm occ}} \epsilon_i$, of the self-consistent (SCF) solution of the Kohn–Sham (KS) Schrödinger equation:

$$\hat{H}_{\rm KS}\psi_i(\mathbf{r}) = \left(-\frac{\hbar^2}{2m_e}\nabla^2 + V_{\rm ion}(\mathbf{r}) + V_{xc}[\rho(\mathbf{r})] + e\int \frac{\rho(\mathbf{r}')}{|\mathbf{r}-\mathbf{r}'|}{\rm d}^3r' \right)\psi_i(\mathbf{r}) = \epsilon_i\psi_i(\mathbf{r}), \quad (2)$$

where $V_{\rm ion}$ is the ionic potential and V_{xc} the exchange-correlation potential.

The second term E_{ee} in equation (1) represents an average electron–electron energy:

$$E_{ee}[\rho(\mathbf{r})] = \frac{e^2}{2}\int \frac{\rho(\mathbf{r})\rho(\mathbf{r}')}{|\mathbf{r}-\mathbf{r}'|}{\rm d}^3r\,{\rm d}^3r', \quad (3)$$

$E_{\text{ion-ion}}$ is the ion–ion interaction energy:

$$E_{\text{ion-ion}} = \frac{e^2}{2}\sum_{i,j}\frac{Z_\alpha Z_\beta}{|\mathbf{R}_\alpha - \mathbf{R}_\beta|}. \quad (4)$$

(Z_α is the nuclear or pseudopotential charge on atom α at position $\vec{R}_\alpha$), and E_{xc} is the exchange-correlation energy.

In the FIREBALL method, a basis set of optimized atomic-like orbitals, $\phi_\mu(\mathbf{r})$, is used to solve equation (2) and to determine the density $\rho(\mathbf{r})$ ($\mu \equiv (\alpha, l, m)$, α is the atomic site, l represents the atomic subshell—e.g. $3s$, $4s$, $3p$, $3d$, etc, and m is the magnetic quantum number); these orbitals are strictly localized in real-space [26, 30]. The computational efficiency of FIREBALL is associated with the possibility to choose $\rho(\mathbf{r})$ in the above equations as a sum of atomic-like densities, $\rho_\alpha(\mathbf{r})$ [27]. In particular, in the FIREBALL approach the electron density $\rho(\mathbf{r})$ is written in terms of the atomic-like orbitals, $\phi_\mu(\mathbf{r})$ as

$$\rho(\mathbf{r}) = \sum_\alpha \rho_\alpha(\mathbf{r}) = \sum_\mu n_\mu |\phi_\mu(\mathbf{r})|^2, \quad (5)$$

where n_μ represents the charge on the orbital ϕ_μ. In this way four-center integrals are not required for the calculation of E_{tot} or the forces $\mathbf{F}_\alpha$, and all the two- and three center interactions are tabulated beforehand and placed in interpolation data-tables which are no larger than 2D [25, 26]. In particular, for the calculation of the exchange-correlation matrix elements different approaches may be used, see [28, 29, 35]; in the calculations presented in section 3 we have used the multicenter weighted exchange-correlation density approximation (McWEDA) [28]. All the matrix elements required during the MD simulation are evaluated by looking up the necessary information from the data-tables (which are read at the beginning of the calculation and stored in memory throughout the MD simulation).

In practice, the atomic densities ρ_α are approximated to be spherically symmetric around each atomic site α (i.e. $n_{\alpha lm} = n_{\alpha lm'}$). Self-consistency is achieved defining output orbital charges n_μ^{out} from the occupied eigenvectors ψ_i of equation (2); and imposing that in the self-consistent solution n_μ^{out} and the input orbital charges n_μ coincide [27]. Different methods can be used to project the output electron density from equation (2) into the form given by equation (5) using for example Löwdin Orbitals [27, 36, 37] or Natural Atomic Orbitals [38].

DFT MD simulations can be performed once the forces

$$\mathbf{F}_\alpha = -\frac{\partial E_{\text{tot}}}{\partial \mathbf{R}_\alpha}. \quad (6)$$

on each atom α are evaluated [26].

2.2. DFT–MDET

In DFT–MDET simulations the atoms follow classical trajectories $\{\mathbf{R}_\alpha(t)\}$ on one of the PESs corresponding to a particular adiabatic state E_{A}. The coupling between the nuclear motion and the electronic quantum state is taken into account by means of probabilistic hops between different adiabatic PESs ($E_{\text{A}} \rightarrow E_{\text{B}}$). The probability for these hops is determined from the time evolution of the electronic states and their non-adiabatic coupling vectors (see below). In the following discussion, we present details about our implementation of the MDET algorithm within the FIREBALL local-orbital DFT code.

The MDET simulation consists of two nested time loops corresponding to the time evolution of the atomic positions and electronic states; the outer time loop corresponds to the atomic motion and the inner time loop to the propagation of the electronic states. The computational procedure consists of 5 algorithm steps (after an initialization step) as shown schematically in figure 1.

Step 1: Solution of the stationary Kohn–Sham Hamiltonian. In this first step we obtain the SCF solution of the stationary KS Hamiltonian for the current atomic configuration and adiabatic state:

$$\hat{H}_{\text{KS}}[\mathbf{R}]\psi_j(\mathbf{r};\mathbf{R}) = \epsilon_j(\mathbf{R})\psi_j(\mathbf{r};\mathbf{R}), \quad (7)$$

where $\mathbf{R}$ represents the atomic positions $\{\mathbf{R}_\alpha(t)\}$ at time t and $\psi_j(\mathbf{r};\mathbf{R})$ are the single-particle adiabatic KS orbitals (at time t). The different adiabatic states, E_{A}, are defined by means of the corresponding set of occupied KS adiabatic orbitals or, in other words, by the occupancies f_k of the ψ_k orbitals, with $f_k = 1$ (occupied) or 0 (empty). For example, the ground state PES is related to the Slater determinant formed by the set of lowest energy occupied adiabatic KS orbitals ψ_k; for the excited states, we assume in the following that the PES are related to singly excited Slater determinants. Thus, the KS Hamiltonian in equation (7) is defined in a selfconsistent way using the occupancies $\{f_k\}$ for the current PES. For this purpose, we perform a *constrained* DFT calculation in which the level occupancy is imposed for a particular PES to maintain the electronic configuration during the SCF cycle. In order to keep track of the identity of the adiabatic KS states at different time steps we calculate the overlaps $\langle\psi_k(t-\Delta t)|\psi_m(t)\rangle$.

Step 2: Calculation of the non-adiabatic couplings. The time evolution of the electronic state is calculated using time-dependent KS theory [39–41]. For this purpose, we expand the time-dependent KS orbitals, φ_i, in terms of the adiabatic KS states

$$\varphi_i(\mathbf{r},t) = \sum_k c_{ik}(t)\psi_k(\mathbf{r};\mathbf{R}), \quad (8)$$

and evolve them using the time-dependent, Schrödinger-like, KS equations:

$$\hat{H}_{\text{KS}}[\mathbf{R}]\varphi_i(\mathbf{r},t) = \mathrm{i}\hbar\frac{\partial\varphi_i(\mathbf{r},t)}{\partial t}. \quad (9)$$

This yields the equations of motion for the coefficients $c_{ik}(t)$ in equation (8):

$$\mathrm{i}\hbar\frac{\partial c_{ik}(t)}{\partial t} = c_{ik}(t)\epsilon_k(\mathbf{R}) - \mathrm{i}\hbar\sum_m c_{im}(t)\mathbf{d}_{km}\cdot\mathbf{V}. \quad (10)$$

In this equation the coupling between the classical motion of the atoms and the time evolution of the electronic quantum state is reflected in the non-adiabatic coupling (NAC) term:

$$\mathbf{d}_{km}\cdot\mathbf{V} \equiv \sum_\alpha \mathbf{d}_{km}^\alpha \mathbf{V}_\alpha, \quad (11)$$

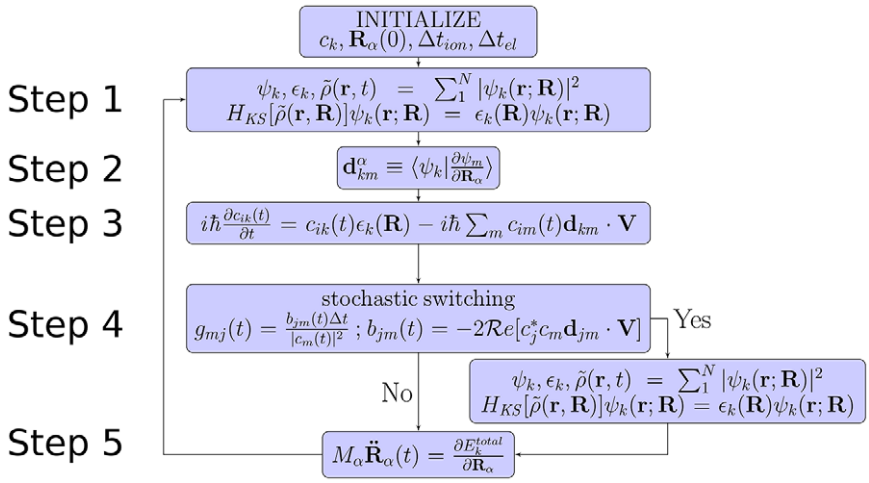

Figure 1. The MDET simulation consists of two nested time loops. Step 1 corresponds to the self-consistent solution of the stationary KS Hamiltonian for the current PES at time t; in step 2 the non-adiabatic coupling term between adiabatic KS states are calculated; step 3 is the inner loop for the time evolution of the electronic states; step 4 corresponds to the fewest switches algorithm: surface hops between different PES are determined using the probabilities g_{mj}; if there is a hop a new self-consistent solution is obtained for the KS Hamiltonian for the new electronic configuration and energy is conserved by means of velocity rescaling along the direction of the NACV; finally in step 5 the atomic positions are updated $t \rightarrow t + \Delta t$ (outer loop).

where $\mathbf{V}_\alpha = \partial\mathbf{R}_\alpha/\partial t$ is the atomic velocity of atom α and $\mathbf{d}^\alpha_{km}$ are the non-adiabatic coupling vectors (NACV) between adiabatic KS states k and m:

$$\mathbf{d}^\alpha_{km} \equiv \langle\psi_k|\frac{\partial\psi_m}{\partial\mathbf{R}_\alpha}\rangle. \tag{12}$$

The NACVs $\mathbf{d}^\alpha_{km}$ are the central quantity for non-adiabatic molecular dynamics. The atomic motion induces changes in the adiabatic states populations $|c_{ik}(t)|^2$ through the coupling of the atomic velocities and the NACVs, see equation (10). Recently, we have derived an expression to calculate the NACVs $\mathbf{d}^\alpha_{km}$ in a basis set of local-orbitals *on the fly* along the MD simulation in a practical and computationally efficient way [42]. Alternatively, the NAC for the time evolution (equation (10)) of the coefficients $c_{ik}(t)$ can be directly calculated using the following numerical derivative [43]:

$$\mathbf{d}_{km}\cdot\mathbf{V} \equiv \langle\psi_k|\frac{\partial\psi_m}{\partial t}\rangle = \frac{1}{2\Delta t}\Big[\langle\psi_k(t-\Delta t)|\psi_m(t)\rangle - \langle\psi_k(t)|\psi_m(t-\Delta t)\rangle\Big], \tag{13}$$

which gives the value of the NAC at time $(t - \Delta t/2)$.

Step 3: Time evolution of the electronic states. Once the NACs have been calculated, we propagate the coefficients c_{ik} from time $(t - \Delta t)$ to time t using a small time step $\Delta t_{\rm el}$ and a 4-th order Runge–Kutta numerical scheme to integrate equation (10). In this numerical solution the quantities used in different electronic time steps $\Delta t_{\rm el}$ are linearly interpolated from the corresponding values for the ionic steps. Typically $\Delta t_{\rm el} \sim \Delta t/500$. This is the inner loop for the propagation of the electronic states for each step, Δt, in the atomic motion.

Step 4: Surface hopping. At each time step Δt, a transition between adiabatic PESs $E_{\rm A} \rightarrow E_{\rm B}$ may occur through a probabilistic 'hop' using the *fewest-switches algorithm* [10]. The MDET algorithm incorporates the following switching probability $g_{jk}(t)$ to define the transition between electronic states $\psi_j \rightarrow \psi_k$ in the time interval $[t - \Delta t, t]$:

$$g_{jk}(t) = \frac{b_{kj}(t)\Delta t}{|c_{jj}(t)|^2}, \tag{14}$$

where the coefficient b_{kj} is defined as:

$$b_{kj}(t) = -2\mathcal{R}e[c^*_{jk}(t)c_{jj}(t)\mathbf{d}_{kj}\cdot\mathbf{V}]. \tag{15}$$

The transitions are determined using a Monte-Carlo approach following the probabilities $g_{jk}(t)$. When a transition takes place, the occupancies of the adiabatic KS orbitals ψ_j and ψ_k are modified: $f_j : 1 \rightarrow 0$; $f_k : 0 \rightarrow 1$, and the stationary KS Hamiltonian, equation (7), is re-calculated for the new electronic configuration (see step 1). In this case, energy conservation is imposed by re-scaling velocities along the direction of the NACV, equation (12) [44, 45]. Hops to higher energy PESs are rejected if insufficient kinetic energy is present. Velocity rescaling and hop rejection ensures detailed balance between transitions up and down in energy. If the switch does not occur, the simulation continues on the current PES.

Step 5: Motion of the atoms. Finally, the atomic positions are updated $\{\mathbf{R}_\alpha(t)\} \rightarrow \{\mathbf{R}_\alpha(t + \Delta t)\}$ using the forces corresponding to the current PES, $E_{\rm A}$:

$$\mathbf{F}_\alpha = -\frac{\partial E_A}{\partial\mathbf{R}_\alpha}; \tag{16}$$

where $\mathbf{F}_\alpha$ is the force acting on atom α. The calculation goes back to step 1, using the new atomic positions. This scheme is repeated until the simulation is finished.

We now describe the parameters used during simulations of photo-cycloaddition (PCA) reactions discussed in the next section. The optimized atomic structure in the ground state is used as the initial molecular configuration for the reactant

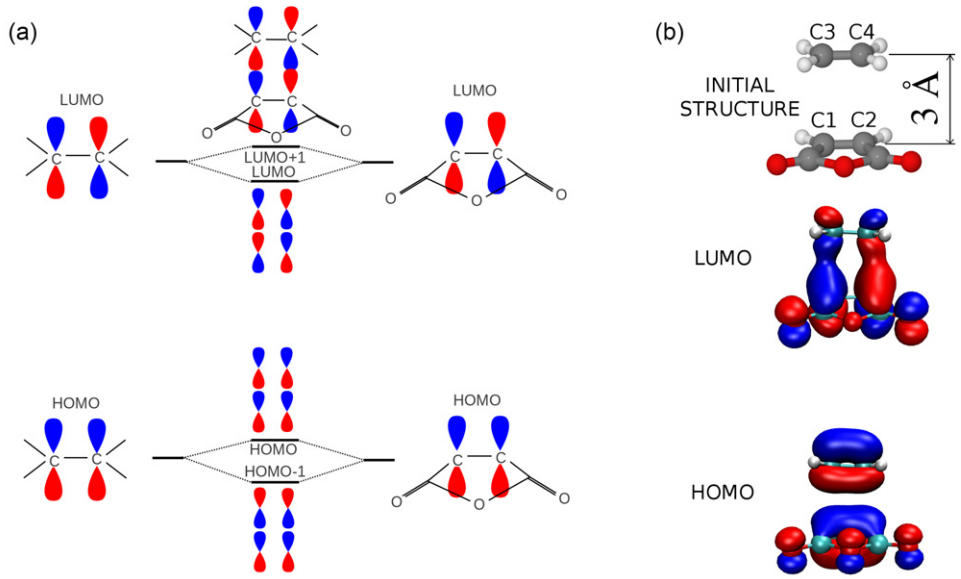

Figure 2. (*a*) Schematic representation of the frontier molecular orbitals involved in the PCA reaction. The figure shows the p_z orbitals associated with the carbon–carbon double bonds in ethylene and maleic anydride. (*b*) (Top) The initial configuration of the reactants. Molecular planes are parallel and displaced 3 Å. (*b*) (Bottom) The HOMO and LUMO Kohn–Sham orbitals for the molecular complex in the initial configuration depicted in real space, showing the intermolecular bonding and anti-bonding character of the LUMO and HOMO, respectively. Red and blue color express positive or negative sign of the wavefunction.

species. Atomic positions of the reactant species were relaxed with convergence criteria for the total energy and forces of 10^{-6} eV and 0.05 eV Å^{-1}, respectively to obtain the optimized structures. All calculations were performed using local density approximation (LDA). The optimized numerical atomic-like orbitals (NAOs) were confined to regions limited by the corresponding cutoff radii r_c [26, 30]. The following r_c for the different NAOs were chosen as follows: hydrogen, $r_c^{\mathrm{H}}(s) = 3.8$ a.u., with an additional s^*-state, $r_c^{\mathrm{H}}(s^*) = 3.8$ a.u.; carbon, $r_c^{\mathrm{C}}(s) = 4.5$ a.u, $r_c^{\mathrm{C}}(p) = 4.5$ a.u., with an additional d-state, $r_c^{\mathrm{C}}(d) = 5.4$ a.u.; and oxygen, $R_c^{\mathrm{O}}(s) = 3.8$ a.u. and $R_c^{\mathrm{O}}(p) = 3.8$ a.u. All molecular dynamics simulations were carried out with the characteristic time steps $t_{\mathrm{ion}} = 0.25$ fs and $t_{\mathrm{el}} = 0.0025$ fs at temperature 500 K and 100 K for maleic anhydride and C_{60}, respectively. Constant temperature molecular dynamics was achieved using an isokinetic NVT thermostat [46].

3. Results: cycloaddition

3.1. Cycloaddition reaction of two small organic molecules: reaction of maleic anhydride with ethylene

To demonstrate the efficiency of our method, we first report DFT–MDET simulations of the photo-cycloaddition (PCA) reaction of maleic anhydride ($C_2O_3H_2$) with ethylene (C_2H_4), forming cyclobutane-1-2-dicarboxilic anhydride ($C_4O_3H_6$), see figure 2(*b*). This PCA reaction is a prototypical reaction frequently encountered in organic chemistry. The reaction is generated by a single electron excitation induced by the interaction with light. During the PCA reaction the two π bonds perish and two σ bonds arise, thus 4 bonding electrons are involved in the reaction process. The frontier molecular orbital description of PCA is schematically presented in figure 2(*a*), where the p_z character of the frontier orbitals, the HOMO and LUMO of the isolated reactants, are displayed on the right and left sides of the figure. The formation of a molecular complex by the two reactants leads to four linear combinations of the frontiers orbitals (shown in center of figure 2(*a*)). Kohn–Sham HOMO and LUMO orbitals in real space for the molecular complex are shown in the bottom of figure 2(*b*). The HOMO orbital is formed by the overlap of π bonds of opposing signs, which gives rise to the intermolecular anti-bonding character of the HOMO orbital, see figure 2(*a*). Consequently, the intermolecular anti-bonding character of the HOMO orbital inhibits a thermally activated reaction. In contrast, the LUMO orbital shows intermolecular bonding characteristics. Thus, a photo-induced electron excitation from the HOMO to the LUMO induces an additional attractive force which facilitates the PCA reaction, as discussed below.

To gain more insight into the reaction mechanisms, we performed, in total, 50 independent DFT–MDET simulations, each with total time of 2 ps; in each simulation, a single electron was initially promoted from the HOMO to the LUMO state of the molecular complex (C_2H_4 + $C_2O_3H_2$). Each simulation took approximately 16 h on single CPU Intel Xeon E5420 @ 2.50 GHz which demonstrates the computational efficiency of our FIREBALL-MDET code. All simulations were initiated from an identical configuration—both planar molecules were oriented parallel and the carbon–carbon double bond (C_3=C_4) of ethylene was positioned above the carbon–carbon double bond (C_1=C_2) of maleic anhydride (see figure 2(*b*) top). The initial distance between the molecular planes of the anhydride and ethylene was 3 Å. The velocities were initialized with a normal distribution corresponding to an initial temperature of 500 K. In order to show clearly the stochastic nature of the MDET algorithm, the same initial positions and velocities were applied for each trajectory. Four frontier orbitals (HOMO-1,

HOMO, LUMO, LUMO + 1) were propagated in time and thus the electron transitions were allowed only amongst these states.

We were able to identify three different deactivation channels of the initial electron excitation according to our simulations: (i) a direct addition reaction of ethylene and the anhydride; (ii) a direct non-reactive de-excitation; and (iii) an intermediate transient state with subsequent de-excitation leading to an addition/dissociation process. According to our simulations, 15, of a total 50, simulations produced the addition reaction forming cyclobutane diacid anhydride; thereby our simulations give an estimated yield of the addition reaction as ≈30%.

A direct addition reaction of reactants was observed in 12 cases. A detailed analysis of the reaction pathway for one of these cases is presented in figure 3. Figure 3(*a*) represents the character in real space of the HOMO and LUMO electronic wave functions at different times along the simulations; in particular the HOMO and LUMO wave functions shown in figure 3(*a*) correspond to the time positions denoted by black vertical lines on figure 3(*b*). The time evolution of the energy spectrum for the four frontiers molecular orbitals with their temporal occupancies is shown in figure 3(*b*). Complementary, figure 3(*c*) shows the PES corresponding to the ground S_0 and first excited S_1 state along the simulation; the cyan dots indicate the actual PES for the simulation. The grey line represents the evolution of the NACV between the HOMO and the LUMO orbitals with its maximum occurring near the conical intersection on figure 3(*c*).

To characterize the pathway of the reaction process, we traced a time evolution of a characteristic distance d_{REAC} and force F_{REAC} acting between reactants. The characteristic distance d_{REAC} measures the distance from the center of ethylene carbon–carbon bond (C_1=C_2, see figure 2) to the center of anhydride carbon–carbon bond (C_3=C_4). We also evaluated the forces acting between the two molecules as $F_{\mathrm{REAC}} = \sum F_{\mathrm{ethylene}} - \sum F_{\mathrm{anhydride}}$ projected along the vector from the center of ethylene carbon–carbon bond to the center of anhydride carbon–carbon bond ($\vec{d}_{\mathrm{REAC}}$). The distance d_{REAC} and force F_{REAC} between reactants are plotted in figure 3(*d*) by the red and blue curves, respectively.

Initially, the HOMO and LUMO have intermolecular anti-bonding and bonding characters, respectively. The partial occupancy of the bonding state (LUMO) induces an attractive force acting between reactants. Consequently their distance d_{REAC} reduces significantly from 3.0 Å to 2 Å. Within ≈60 fs the system approaches towards the region of the conical intersection and the HOMO and LUMO exchange their characters—the HOMO is now a bonding orbital and vice versa. In this particular case, after the 'crossing' of the HOMO and LUMO, a de-excitation of the electron from LUMO (anti-bonding) to HOMO (bonding) happens at approximately 86 fs, which stabilizes the final molecular complex and produces the addition reaction. The force F_{REAC} becomes strongly attractive, driving the system to the final bound state with the distance d_{REAC} oscillating around 1.6 Å.

We should note that, in this particular case, the switching mechanism does not occur at the distance with the NACV

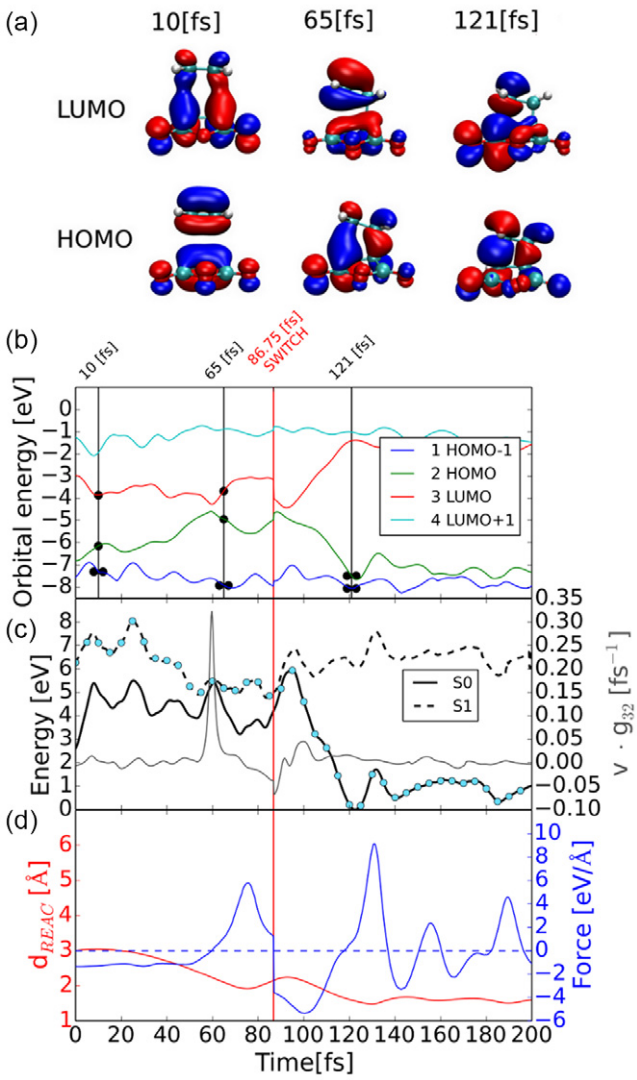

Figure 3. Analysis of a direct addition reaction of ethylene and maleic anhydride. (*a*) Character in real space of HOMO and LUMO electronic wave functions corresponding to the time points indicated by black vertical lines on graph (*b*). (*b*) Energy spectra for the four frontier molecular orbitals; the black dots indicate the electron occupancies of the different states. (*c*) Potential energy surfaces corresponding to the ground S_0 and first excited S_1 state together with the nonadiabatic coupling term $\mathbf{d}_{ij} \cdot \mathbf{V}$ between HOMO and LUMO (solid grey line); the cyan dots indicate the actual PES for the simulation. (*d*) Distance between the center of ethylene carbon–carbon bond (C_1–C_2) to the center of maleic anhydride carbon–carbon bond (C_3–C_4) (red) and forces acting between reactants (blue).

maximum, but later due to the stochastic nature of the fewest switches MDET procedure. In other trajectories we observe a LUMO to HOMO electron transition near the crossing region. In these cases the electronic transition from LUMO to HOMO happens at approximately 61 fs, very near to the conical intersection, with the HOMO exhibiting am intermolecular bonding character. After this transition, the PCA reaction is completed.

The second deactivation channel consists of the direct nonreactive de-excitation. In our simulations, we have detected 13 cases (out of 50) of the direct dissociation. In these

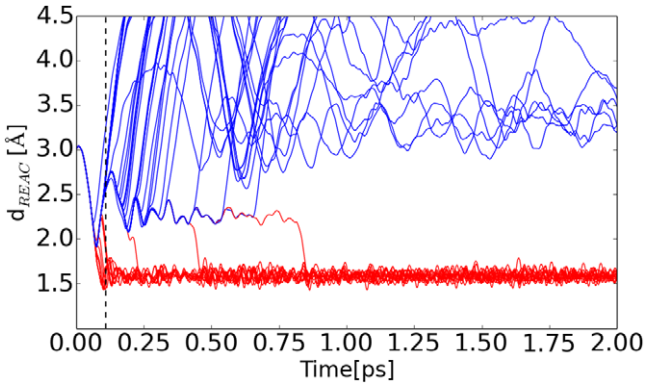

Figure 4. Time evolution of the characteristic distance d_{REAC} measured between the center of ethylene carbon carbon bond (C_1–C_2) to the center of anhydride carbon carbon bond (C_3–C_4) for the 50 DFT–MDET simulations. Red curves represent the cases when the addition reaction occurred and the blue curves represent the dissociation processes. A direct addition reaction takes place in 12 cases; in 3 other cases the addition reaction was found to occur through a transient intermediate state.

cases, the system evolves initially along the same trajectory as in the previous cases.The electron hopping occurs between the LUMO and the HOMO at 104 fs, where HOMO and LUMO have anti-bonding and bonding characteristics, respectively, similar to the initial configuration, which leads to a double occupancy of the intermolecular anti-bonding HOMO state; this induces an important change in the force between both molecules, that after the transition presents a large repulsive value (2 eV Å^{-1}), driving the molecules far from each other. Thus, the addition reaction is not produced.

The third deactivation channel is related with the formation of an intermediate state which is characterized by the formation of just one carbon–carbon bond between maleic anhydride and ethylene. In this intermediate state the distance d_{REAC} oscillates around 2.3 Å as shown on figure 4. In this case the system typically finalizes (22 cases out of 50) in the decoupling of the molecular reactants but we detected 3 cases where the intermediate case produces the complete addition reaction (see figure 4).

3.2. Polymerization of two C_{60} molecules via cycloaddition

Here, as a second example of the application of our FIREBALL-MDET code, we present simulations of the polymerization process of two free-standing C_{60} molecules via a 2 + 2 PCA reaction. This reaction was first reported by Rao *et al* in 1993 [47]. The basic principles for this case are similar to our discussion in the previous section, see figure 2. Accordingly, the HOMO of the molecular complex C_{60}–C_{60} has an intermolecular anti-bonding character while the bonding character is mainly associated to the LUMO + 1 orbital (see figure 5(*c*)). We should note that the LUMO and LUMO + 1 orbitals are nearly degenerate with an energy difference of 0.08 eV in the initial configuration. Nevertheless the LUMO+1 shows a strong bonding character with pronounced electron densities localized between the frontiers atoms of the two C_{60} molecules.

Here we consider the case where two C_{60} molecules are oriented by 56/65 edges (see figure 5(*b*)) against each other [48]. In the first step, we examine the PESs as a function of distance between the two C_{60} molecules in the ground S_0, first excited S_1, and second excited S_2 states for distances in the range from 1.3 to 3.0 Å, with incremental changes in the distance of 0.05 Å. In this calculations we fixed z and y coordinates of the four interacting carbon atoms forming the 56/65 edge see figure 5(*b*), i.e. those involved in the cycloaddition chemical bond, and the rest of the atomic positions were allowed to relax. The calculated PES S_0, S_1 and S_2 are plotted in figure 5(*a*). We can identify two minima on the S_0 PES: (i) a global one located at the distance of ≈2.69 Å, which corresponds to two weakly interacting C_{60} molecules; (ii) and the second, a local minimum found at the distance of ≈1.56 Å. This second minimum corresponds to two chemically bonded C_{60} molecules. In between these two energy minima, there is an energy barrier of ≈0.6 eV located at a distance of 1.75 Å, which avoids a spontaneous transition from the energetically higher chemically bound state to the weakly bound state. At this distance there is a conical intersection between S_0 and S_1.

Figure 5(*a*) also shows the ground state PES as calculated with the AIMS code [49] (which employs high-accuracy numerical orbitals and thus allows better sampling of the Hilbert space). This PES is quite similar to our result; in particular, the conical intersection is found at the same distance, 1.75 Å.

In our DFT–MDET simulations, we initially placed two C_{60} molecules at a distance of 2.0 Å (vertical line in figure 5(*a*)) i.e. 0.25 Å away from the conical intersection, and one electron was promoted from the HOMO to the LUMO+1 state. During the simulation, we let the system evolve in time for 0.5 ps at a constant temperature of 100 K, with initial velocities chosen as discussed in the previous section. Electron transitions are allowed between three orbitals—HOMO, LUMO and LUMO + 1. Our simulations identify two scenarios: (i) a PCA reaction forming a C_{60} bonded dimer; or (ii) a complete decoupling of the two C_{60} molecules towards the weakly bound minimum. In total, we carried 20 trajectories and 3 of the simulations yielded the polymerization process; 17 simulations lead to the separation of the C_{60} molecules.

Figure 6 shows the time evolution for a case where electron de-excitation happens via the 2 + 2 cycloaddition reaction. Figure 6(*a*) represents the HOMO, LUMO and LUMO + 1 KS orbitals at three different snapshots corresponding to the vertical black lines in figure 6(*b*). Figure 6(*b*) shows the time evolution of the HOMO, LUMO and LUMO + 1 KS eigenvalues. Figure 6(*c*) shows the PESs corresponding to the ground S_0, first S_1 and second S_2 excited states throughout the simulation. The cyan circles identify on which PES the system is located at a given time during the simulation. The solid/dashed grey line represents the evolution of the NACVs between the LUMO and HOMO and between the LUMO + 1 and LUMO, respectively. Finally, figure 6(*d*) displays the evolution of the force F_{REAC} acting between the two molecules and their distance d_{REAC}, which is defined as an average distance between the frontiers atoms on the 56/65 edges of each

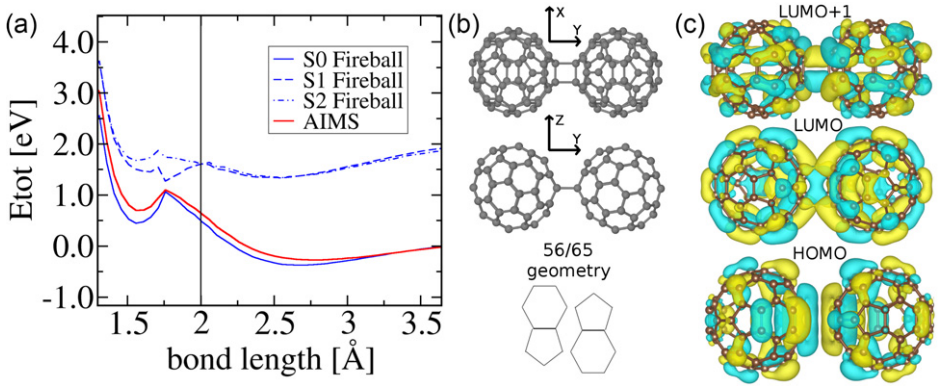

Figure 5. (*a*) Potential energy surfaces of the PCA reaction between 2 fullerenes: ground state S = 0 (solid line), first-excited state S_1 (dashed line) and second excited state S_2 (dot–dashed line), ground state PES calculated using AIMS code [49] (red solid line). (*b*) Atomic structure of the fullerene dimer of 56/65 geometry. (*c*) Real space representation of HOMO, LUMO and LUMO + 1 KS electronic wave functions for the initial configuration (vertical line in (*a*)). While the HOMO orbital has intermolecular anti-bonding character, LUMO + 1 is bonding.

molecule. Similarly, the force F_{REAC} is the difference between the sum of forces acting on each C_{60} molecule projected along the vector d_{REAC}.

Initially, the S_1 and S_2 states are almost degenerate, see figure 6(*c*). Very rapidly in the simulation, the LUMO and LUMO + 1 energy states show a strong mixing and a large NACV, and an electronic hopping between LUMO + 1 and LUMO occurs (at $t = 4.75$ fs). The system evolves now in the S_1 excited state and the LUMO and LUMO + 1 energy levels move away from each other. The LUMO orbital (occupied by one electron) has now the stronger intermolecular bonding character, see figure 6(*a*) ($t = 23$ fs). As shown in figure 6(*d*), in this part of the trajectory there is a repulsive force F_{REAC} between the two C_{60} molecules but the distance d_{REAC} decreases. A detailed analysis of the motion of the system shows that while most of the carbon atoms in each molecule move away from the other molecule, the two frontiers atoms on each molecule actually approach closer towards the two frontier atoms on the other molecule due to the excited electron in the bonding LUMO orbital. Consequently, both C_{60} molecules tend to elongate. The repulsive force F_{REAC} and the distance d_{REAC} diminish in time and the system evolves towards a conical intersection between S_0 and S_1, which increases the NACV between the HOMO and LUMO. The proximity of the conical intersection induces an electron switching between the LUMO and HOMO. After this transition the HOMO and LUMO exchange their bonding and anti-bonding characters. Now, the bonding HOMO has two electrons and the anti-bonding LUMO is empty. Consequently, strong chemical bonds are established between the frontier carbon atoms and the PCA reaction is completed. In the remaining simulation time the distance d_{REAC} oscillates around its equilibrium position while all the carbon atoms relax in a complex way to minimize the initial elongation.

An example of the non-reactive pathway is presented in figure 7. Initially, the system evolves very similarly to the previous case where the system appraoches a conical intersection between S_1 and S_2; due to the probabilistic nature of the fewest switches method, the electronic transition from LUMO + 1 to LUMO takes place now a little later, at $t = 5.75$ fs, see figure 7(*b*). The system evolves then in the S_1 state, moving towards a S_0–S_1 conical intersection, but the electron hopping does not occur now. Thus, the systems stays in the S_1 PES, with a repulsive force F_{REAC} acting between both molecules; the distance d_{REAC} oscillates (figure 7(*d*)), due to the attraction associated with the bonding LUMO (occupied with one electron), see figure 7(*a*). During the second oscillation cycle, when d_{REAC} decreases again the S_1 and S_0 PESs (and the LUMO and HOMO energy levels) approach each other again and the electron hop takes place now, at time $t = 100$ fs (figure 7(*b*) and (*c*)). The HOMO (occupied by two electrons) presents an intermolecular anti-bonding character now (see figure 7(*a*), $t = 110$ fs), enhancing the repulsive force F_{REAC}. Consequently the distance d_{REAC} increases and the system goes to the weakly interacting ground state (figure 5) and the PCA reaction does not occur.

4. Conclusions

The computational simulation of photo-induced processes in large molecular systems is a very challenging problem. Here, we have presented a detailed description of our implementation of a DFT–MDET technique within our local-orbital code FIREBALL, suitable for the computational study of these problems. The MDET technique consists of two nested time loops: an outer loop for the motion the atoms and an inner loop for the propagation of the electronic states. The atoms move in adiabatic PESs, that are calculated using constrained DFT calculations for the different electronic configurations. The time evolution of the electronic states is calculated using time-dependent KS theory. The coupling of the atomic motion and the time evolution of the electronic states is taken into account by means of probabilistic hops between different PESs, using the fewest switches algorithm. When hops take place, energy conservation is imposed re-scaling the velocities along the direction of the non-adiabatic coupling vectors, that are calculated on the fly along the molecular dynamics simulation [42].

As an example of the application of this DFT–MDET approach, we have presented some simulations for two

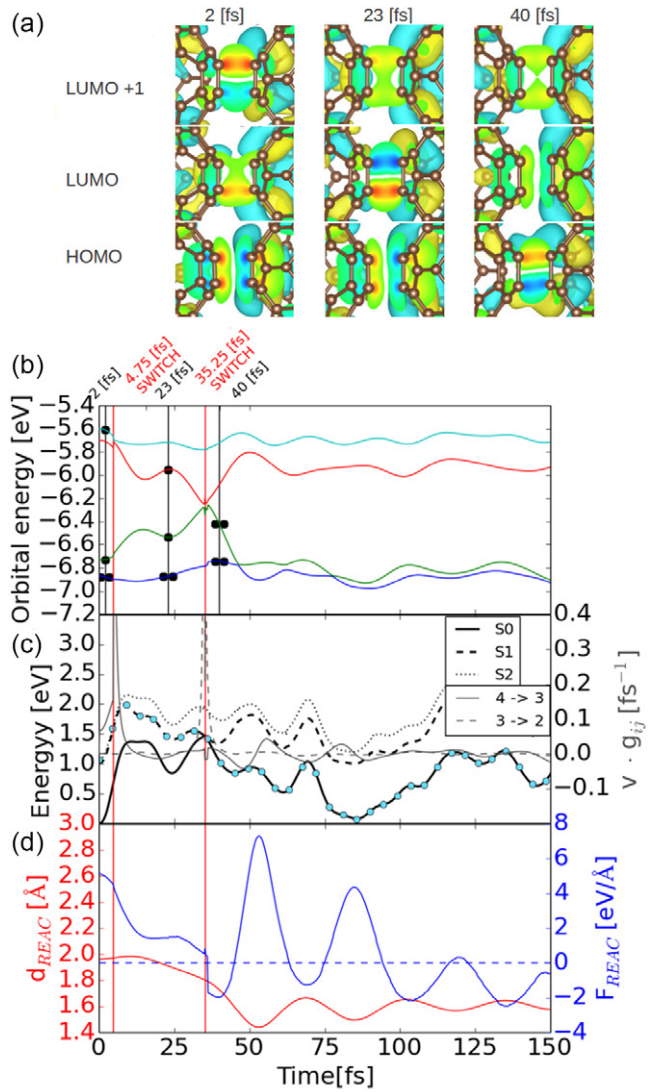

Figure 6. (*a*) Real space representation of HOMO, LUMO and LUMO + 1 KS orbitals corresponding to the time points indicated by the black vertical lines on graph (*b*). (*b*) Energy spectra of four frontier molecular orbitals. (*c*) Potential energy surfaces corresponding to the S_0, S_1 and S_2 states together with the nonadiabatic coupling terms $\mathbf{d}_{ij} \cdot \mathbf{V}$ (solid grey line: between LUMO + 1 and LUMO, dashed grey line: between LUMO and HOMO); the cyan dots indicate the actual PES for the simulation. (*d*) Distance between the center of two reacting carbon atoms of the first fullerene to the center of the two reacting carbon atoms of the second fullerene (red) and forces acting between both molecules (blue).

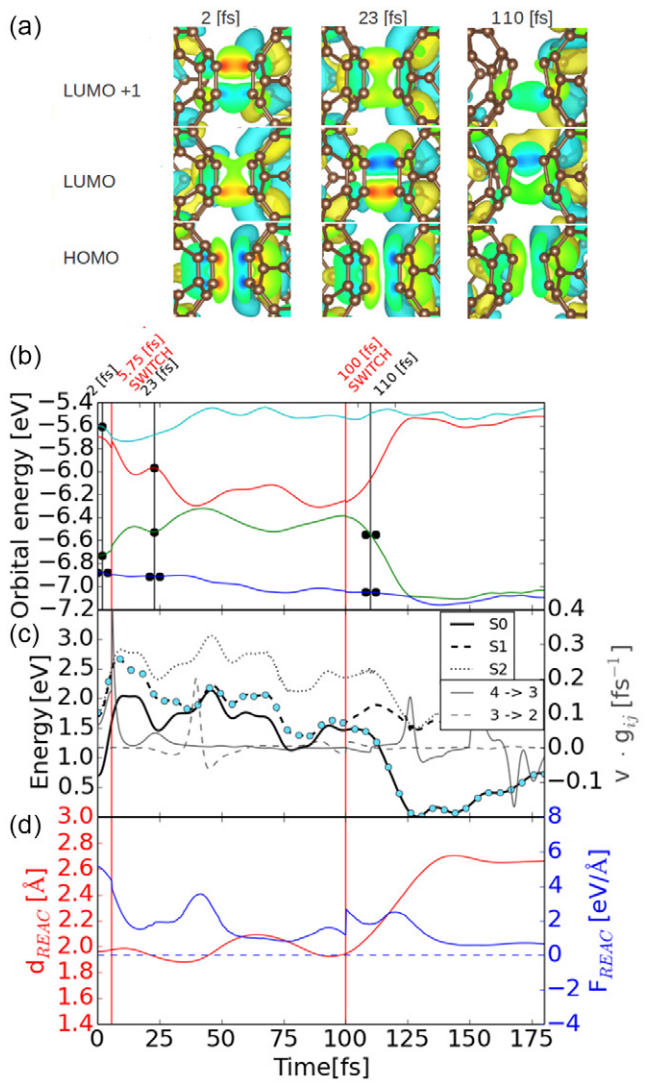

Figure 7. (*a*) Real space representation of HOMO, LUMO and LUMO + 1 KS orbitals corresponding to the time points indicated by the black vertical lines on graph (*b*). (*b*) Energy spectra of four frontier molecular orbitals. (*c*) Potential energy surfaces corresponding to the S_0, S_1 and S_2 states together with the nonadiabatic coupling terms $\mathbf{d}_{ij} \cdot \mathbf{V}$ (solid grey line: between LUMO + 1 and LUMO, dashed grey line: between LUMO and HOMO); the cyan dots indicate the actual PES for the simulation. (*d*) Distance between the center of two reacting carbon atoms of the first fullerene to the center of the two reacting carbon atoms of the second fullerene (red) and forces acting between both molecules (blue).

different photo-induced cycloaddition reactions: the reaction of two small organic molecules (maleic anhydride and ethylene, forming cyclobutane-1-2-dicarboxilic anhydride) and the polymerization reaction of two C_{60} molecules. In the first case, an electron is initially promoted from the HOMO to the LUMO; the LUMO presents an intermolecular bonding character, inducing an attractive force between both molecules. At a time of ∼60 fs, the system goes through a S_1–S_0 conical intersection, with a large value of the NACV between HOMO and LUMO. We identify three different deactivation channels of the initial electron excitation, depending on the time of the electronic transition from LUMO to HOMO, and the character of the HOMO after the transition. In particular, the cycloaddition reaction is established when the HOMO is an intermolecular bonding state after the transition. In the case of the larger C_{60} molecules, the S_1 and S_2 states are initially almost degenerate and we promote one electron from the HOMO to the LUMO + 1. Very rapidly in the simulations (∼5 fs) the electron hops from the LUMO + 1 to the LUMO and the system evolves in the S_1 state towards a S_1–S_0 conical intersection. In this part of the simulations there is an overall repulsive force between both molecules and an attractive force between the frontier atoms on each molecule due to the excited electron in the bonding LUMO state; thus, the molecules tend

to elongate. We identify two different scenarios, depending on the time of the electronic transition from LUMO to HOMO and the character of the HOMO state after the transition: (i) a PCA reaction forming a bonded C_{60} dimer; and (ii) the motion of the system towards the weakly coupled ground state.

Acknowledgments

This work is supported by the Spanish MICIIN (project FIS2010-16046). VZ, PH and PJ acknowledge the support by GAČR, grant no. 14-02079S. This work is supported by the project DE-SC0004737 from the Department of Energy.

References

[1] Keal T W, Koslowski A and Thiel W 2007 Comparison of algorithms for conical intersection optimisation using semiempirical methods *Theor. Chem. Acc.* **118** 837–44
[2] Bearpark M J, Robb M A and Bernhard Schlegel H 1994 A direct method for the location of the lowest energy point on a potential surface crossing *Chem. Phys. Lett.* **223** 269–74
[3] Manaa M R and Yarkony D R 1993 On the intersection of two potential energy surfaces of the same symmetry. Systematic characterization using a Lagrange multiplier constrained procedure *J. Chem. Phys.* **99** 5251
[4] Yarkony D R 2004 Marching along ridges. Efficient Location of energy-minimized conical intersections of two states using extrapolatable functions *J. Phys. Chem.* A **108** 3200–5
[5] Rössle S, Friedrichs J and Frank I 2010 The formation of DNA photodamage: the role of exciton localization *ChemPhysChem* **11** 2011–5
[6] Doltsinis N L 2002 *Quantum Simulations of Complex Many-Body Systems: From Theory to Algorithms* ed J Grotendorst *et al* (Jülich: NIC)
[7] Barbatti M 2011 Nonadiabatic dynamics with trajectory surface hopping method *Wiley Interdiscip Rev.: Comput. Mol. Sci.* **1** 620–33
[8] Curchod B F E, Rothlisberger U and Tavernelli I 2013 Trajectory-based nonadiabatic dynamics with time-dependent density functional theory *ChemPhysChem* **14** 1314–40
[9] Doltsinis N L 2006 Molecular dynamics beyond the born-oppenheimer approximation: mixed quantum classical approaches *Computational Nanoscience: Do It Yourself!* vol 31 (Jülich: NIC) pp 389–409
[10] Tully J C 1990 Molecular dynamics with electronic transitions *J. Chem. Phys.* **93** 1061
[11] Tully J C and Preston R L 1971 *J. Chem. Phys.* **55** 562
[12] Doltsinis N L and Marx D 2002 Nonadiabatic car-parrinello molecular dynamics *Phys. Rev. Lett.* **88** 166402
[13] Craig C F, Duncan W R and Prezhdo O V 2005 Trajectory surface hopping in the time-dependent Kohn-Sham approach for electron-nuclear dynamics *Phys. Rev. Lett.* **95** 163001–5
[14] Duncan W R and Prezhdo O V 2008 Temperature independence of the photoinduced electron injection in dye-sensitized TiO_2 rationalized by *ab initio* time-domain density functional theory *J. Am. Chem. Soc.* **130** 9756–62
[15] Habenicht B F and Prezhdo O V 2008 Nonradiative quenching of fluorescence in a semiconducting carbon nanotube: a time-domain *ab initio* study *Phys. Rev. Lett.* **100** 197402–6
[16] Tapavicza E, Tavernelli I and Rothlisberger U 2007 Trajectory surface hopping within linear response time-dependent density-functional theory *Phys. Rev. Lett.* **98** 023001
[17] Tavernelli I, Tapavicza E and Rothlisberger U 2009 Nonadiabatic coupling vectors within linear response time-dependent density functional theory *The J. Chem. Phys.* **130** 124107
[18] Tapavicza E, Bellchambers G D, Vincent J C and Furche F 2013 *Ab initio* non-adiabatic molecular dynamics *Phys. Chem. Chem. Phys.* **15** 18336–48
[19] Neukirch A J, Shamberger L C, Abad E, Haycock B J, Wang H, Ortega J, Prezhdo O V and Lewis J P 2014 Nonadiabatic ensemble simulations of cis-stilbene and cis-azobenzene photoisomerization *J. Chem. Theory Comput.* **10** 14–23
[20] Mitric R, Werner U, Wohlgemuth M, Seifert G and Bonacic-Koutecky V 2009 Nonadiabatic dynamics within time-dependent density functional tight binding method *J. Phys. Chem.* A **113** 12700–5
[21] Lan Z, Lu Y, Fabiano E and Thiel W 2011 QM/MM nonadiabatic decay dynamics of 9h-adenine in aqueous solution *ChemPhysChem* **12** 1989–98
[22] Wohlgemuth M, Bonacic-Koutecky V and Mitric R 2011 Time-dependent density functional theory excited state nonadiabatic dynamics combined with quantum mechanical/molecular mechanical approach: photodynamics of indole in water *J. Chem. Phys.* **135** 054105
[23] Tapavicza E, Meyer A M and Furche F 2011 Unravelling the details of vitamin d photosynthesis by non-adiabatic molecular dynamics simulations *Phys. Chem. Chem. Phys.* **13** 20986–98
[24] Malis M *et al* 2012 Unraveling the mechanisms of nonradiative deactivation in model peptides following photoexcitation of a phenylalanine residue *J. Am. Chem. Soc.* **134** 20340–51
[25] Lewis J P *et al* 2011 Advances and applications in the fireball *ab initio* tight-binding molecular-dynamics formalism *Phys. Status Solidi* B **248** 1989–2007
[26] Sankey O F and Niklewski D J 1989 *Ab initio* multicenter tight-binding model for molecular-dynamics simulations and other applications in covalent systems *Phys. Rev.* B **40** 3979–95
[27] Demkov A A, Ortega J, Sankey O F and Grumbach M P 1995 Electronic structure approach for complex silicas *Phys. Rev.* B **52** 1618–30
[28] Lewis J P, Glaesemann K R, Voth G A, Fritsch J, Demkov A A, Ortega J and Sankey O F 2001 Further developments in the local-orbital density-functional-theory tight-binding method *Phys. Rev.* B **64** 195103
[29] Jelínek P, Wang H, Lewis J P, Sankey O F and Ortega J 2005 Multicenter approach to the exchange-correlation interactions in *ab initio* tight-binding methods *Phys. Rev.* B **71** 235101
[30] Basanta M A, Dappe Y J, Jelínek P and Ortega J 2007 Optimized atomic-like orbitals for first-principles tight-binding molecular dynamics *Comput. Mater. Sci.* **39** 759–66
[31] Schwarz K W 1985 Three-dimensional vortex dynamics in superfluid ^{4}He: line–line and line-boundary interactions *Phys. Rev.* B **31** 5782–804
[32] Matthew C W and Haydock R 1989 Tight-binding models and density-functional theory *Phys. Rev.* B **39** 12520–36
[33] García-Vidal F J, Merino J, Pérez R, Rincón R, Ortega J and Flores F 1994 Density-functional approach to lcao methods *Phys. Rev.* B **50** 10537–47
[34] Schönhammer K, Gunnarsson O and Noack R 1995 Density-functional theory on a lattice: Comparison with exact numerical results for a model with strongly correlated electrons *Phys. Rev.* B **52** 2504

[35] Horsfield A P 1997 Efficient *ab initio* tight binding *Phys. Rev.* B **56** 6594–602
[36] Löwdin P 1950 No Title *J. Chem. Phys.* **18** 365
[37] Carlson B C and Keller J M 1957 Orthogonalization procedures and the localization of wannier functions *Phys. Rev.* **105** 102–3
[38] Reed A E, Weinstock R B and Weinhold F 1985 Natural Population analysis *J. Chem. Phys.* **83** 735
[39] Runge E and Gross E K U 1984 *Phys. Rev. Lett.* **52** 997
[40] Marques M A L and Gross E K U 2004 *Annu. Rev. Phys. Chem.* **55** 427–55
[41] Craig C F, Duncan W R and Prezhdo O V 2005 *Phys. Rev. Lett.* **95** 163001
[42] Abad E, Lewis J P, Zobać V, Hapala P, Jelinek P and Ortega J 2013 Calculation of non-adiabatic coupling vectors in a local-orbital basis set *J. Chem. Phys.* **138** 154106
[43] Hammes-Schiffer S and Tully J C 1994 Proton transfer in solution: molecular dynamics with quantum transitions *J. Chem. Phys.* **101** 4657
[44] Coker D F and Xiao L 1995 Methods for molecular dynamics with nonadiabatic transitions *J. Chem. Phys.* **102** 496–510
[45] Herman M F 1984 Nonadiabatic semiclassical scattering. I. Analysis of generalized surface hopping procedures *J. Chem. Phys.* **81** 754–63
[46] Evans D J, Hoover W G, Failor B H, Moran B and Ladd A J C 1983 Nonequilibrium molecular dynamics via gauss's principle of least constraint *Phys. Rev.* A **28** 1016–21
[47] Rao A M *et al* 1993 Photoinduced polymerization of solid C_{60} films *Science* **259** 955–7
[48] Strout D L, Murry R L, Xu C, Eckhoff W C, Odom G K and Scuseria G E 1993 A theoretical study of buckminsterfullerene reaction products: $C_{60} + C_{60}$ *Chem. Phys. Lett.* **214** 576–82
[49] Blum V, Gehrke R, Hanke F, Havu P, Havu V, Ren X, Reuter K and Scheffler M 2009 *Ab initio* molecular simulations with numeric atom-centered orbitals *Comput. Phys. Commun.* **180** 2175